Diyala Journal of Engineering Sciences

Journal homepage: https://djes.info/index.php/djes

ISSN: 1999-8716 (Print); 2616-6909 (Online)

Laser Cladding Treatment to Enhance the Corrosin Resistance and Surface Hardness by Electrophoretic Coatings to A283 Steel

Shahbaa Ahmed Albayati [1,2], Ali Bahari [1], H. A. Hussien [3], Haneen M Alsafi[4*], Ali Aljelif[2], Mahdi Mousavi[5], Sanaz Soufian[5] and Ayad Naseef Jasim[6]

[1] Department of solid-state physics, University of Mazandaran, Iran
[2] Ministry of oil, Baghdad - Iraq
[3] Production Engineering and Metallurgy Department, University of Technology, Baghdad-Iraq
[4] Institute of Natural Sciences and Mathematics Ural federal Russian Federation.
[5] Novian Laser Saba company-Esfahan, Iran
[6] Department of Materials Engineering, University of Diyala, 32001 Dyala-Iraq

ARTICLE INFO

Article history:
Received September 14, 2022
Accepted October 12, 2022

Keywords:
Laser cladding
Corrosion resistance
Surface treatment
Al_2O_3 alloying

ABSTRACT

Laser cladding (LC) is a laser-based surface modification technology that has been widely adopted for the development of thin layers that operate under harsh conditions. Corrosion contributes to approximately 50% of oil and refinery equipment failures. These major risks require sophisticated methods to improve oil equipment performance. LC promotes the generation of superior properties on the substrate surface, which improves service life. To reduce corrosion failure and enhance life cycles, we conducted electrophoretic deposition (EPD) of Ti and Ni powders and directly coated them on A283 steel alloy, which was alloyed by ND-YAG LC and the remelted surface of A283 steel alloy. The microstructure, element distribution and phase analysis of the cladding sample were studied by optical microscopy, field-emission scanning electron microscopy, X-ray energy-dispersive spectrometry, atomic force microscopy and X-ray diffraction methods. The results indicated that the coatings with fine metallurgical bonding to the substrate comprised major stable FeTi and FeNi and illustrated two different regions of solidification microstructures. The LC process and powder feeding by EPD were applied, which improved the mechanical properties, corrosion behaviour, phase transformation and structural optimisation of the surface microstructure of the laser mixed zone. Melting of the coated sample showed that the coating produced by laser treatment had a smooth top surface. In addition, we have a proven case of surface treatment with a laser that delivered the required performance. Moreover, this treatment is a more environmentally friendly alternative to traditional surface preparation treatments.

1. Introduction

Various alternatives to surface treatment through laser-aided material processing have been developed over the last two decades [1]. The industry has been encouraged to use laser surface treatments to improve the corrosion resistance and surface hardening of metal alloys in a more efficient manner than traditional methods due to rapid advancements in the field of laser pulse generation [2,3]. Laser surface processing is an effective method for improving the surface properties of metal alloys. This technique was employed as a purely mechanical and corrosion surface treatment in the early stages of laser processing [4,5].

The thermo-mechanical effect of laser surface treatment by Nd:YAG laser, whose wavelength is shorter than 355 nm, is a

* Corresponding author.
E-mail address: 70082@uotechnology.edu.iq
DOI: 10.24237/djes.2022.15405

preventive maintenance technique for corrosion in oil pipelines [6]. According to the literature, external factors include temperature [7], pH, moisture [8] and salts. In addition, chemical conditions, including particle velocity [9], alloy composition [10] and chemicals [11], are important factors in the external corrosion of pipelines buried in soil. The environment's aggression is heightened by flowing conditions, especially when sand is present. Flow can potentially breach any protective or semi-protective corrosion product layers and increase mass transfer rates along the pipe wall [12]. More corrosion issues are predicted in the future because wells age with the increase in water and sand. Various types of test rigs have been developed over the years to simulate corrosion failure processes in the industry. Zeng [13] used electrode array techniques to investigate the erosion–corrosion behaviour of X65 carbon steel elbows. The percentages of four types of damage (pure corrosion and corrosion-enhanced erosion) were calculated to reveal the dominant factors in corrosion at various locations in the elbow. Zumofen's [14] experiments used 30CrNiMo8 powder, which was successfully laser processed at a percentage of 99.5%, resulting in good mechanical characteristics. High cooling rate and tempering produced a more homogeneous microstructure than the built-up casing [14, 15]. The literature reported laser treatments of different types of alloys, with consideration of the internal and external effects of metals on various environments [7,12]. This research used laser Nd:YAG for surface treatments of A283c processed by nano-coating via electrophoretic deposition (EPD).

2. Methodology

2.1 Preparation of specimens

The A283 steel with a low carbon with composition (Table 1) was used as a substrate. Specimens (50×30×5 mm^3) were cut from the sheet and prepared. The surface roughness was adjusted to Ra 22.44 µm using sand-blasted TiO_2 abrasive with a particle size of 250 µm. Then, the specimens were rinsed with ethanol and ultrasonically cleaned for 10 min. Next, the samples were dipped in HCl 20% for 10 min to remove oxide layers from the substrate. Finally, the metal was rinsed thoroughly with distilled water prior to deposition (Figure 1).

Table 1: Chemical composition (wt. %) of Al-Si alloy used in this study

Fe	C	Si	Mn	P	S	Cr	Ni	Mo	Element
Bal.	0.23	0.171	0.402	0.032	0.012	0.024	0.012	0.002	Content wt. %

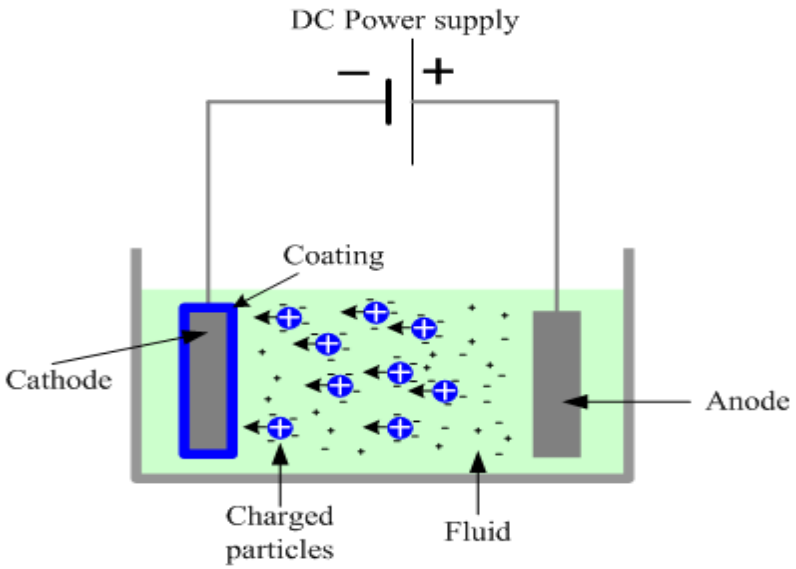

Figure 1. Schematic of the electrochemical deposition (EPD)

2.2 Electrophoretic deposition and suspension preparation

EPD was carried out in a suspension prepared by two-time dispersion of 1 g (A) Al_2O_3 with 10% Ni and TiO_2 with 10% Ni nanopowder and 0.005% iodine dissolved in 100 mL ethanol 99.8% purity. The suspension was stirred by magnetic string for 24 h. The nano powder was characterised by an average particle size of 20–50 nm. The suspensions were obtained via ultrasonic mixing for 40 min at room temperature. The A283 steel substrate was used as a cathode and 304 steel as a counter electrode. The electrodes were placed in parallel with each other within a distance of 10 mm and connected to a DC power source. The EPD was performed at a voltage of 40 V for 5 min at 30 °C. Finally, it was air-dried at room temperature for 24 h.

2.3 Laser Treatment

The second stage was the protection and enhancement of the alloying surface of A283 steel by laser cladding (LC) treatment (model VAIO-NLS-5w). Table 2 shows the optimum processing parameters and laser models used for LC coatings during EPD, which applied ceramic, metals and mixed metals and ceramic with desired porosity and thickness as a sacrificial layer overlay and/or an impermeable layer through controlled laser parameters.

Table 2: Processing parameters for laser cladding coatings on A283

Model	**VAIO-NLS-5w**
Laser source	DPSS/Nd: YVO4
Laser wavelength	355 nm
Average laser power	5 W
Maximum pulse energy	0.2 mj @30 kH
Peak power	13 kW
Pulse repetition frequency	15-100 kHz
Pulse width	<15 ns @ 30 kH
Beam quality	TEM00(M2<1.05)
M2 < 1.05 Polarization	100:1
Beam circularity	>90%
Marking area	Up to 300 mm * 300 mm
Marking speed	14000 mm/s
Minimum line width	5 ~ m
Minimum character	0.02 mm
Cooling system	Water-cooling
Electrical requirements 220 v/50 Hz	800 W
Dimensions	695 * 166 * 160 mm

2.4 Metallographic studies
2.4.1 Structure and morphology of coatings

Preparation of samples for microstructural examination mainly involved sampling, grinding, polishing and etching. The samples were filed and ground. Grinding was conducted in sequence on a roll grinder using silicon carbide abrasive papers with 220, 320, 400 and 600 grits. Polishing and final polishing were performed using a paste made from silicon carbide powder with 1000 grit. The polishing process was applied on the samples using diamond paste with a size of 1 µm, a special polishing cloth and lubricant. The samples were cleaned with a mixture of water and alcohol and dried with hot air. Then, the samples were examined using a Nikon ME-600 optical

microscope equipped with a NIKON camera (DXM-1200F).

Surfaces and cross sections of the coatings were observed using high-resolution field-emission scanning electron microscopy (FE-SEM, INSPECT F50). The chemical composition of the coatings was investigated using X-ray energy-dispersive spectrometry (EDS). Phase identification was performed using X-ray diffraction (Bruker AXS, D8) with monochromatised CuKα radiation and a scan rate of 0.02°/s within a 2Θ range of 10–90°. Atomic force microscopy (AFM) is a characterisation technique at the micro- or nano-scale. Knowing surface roughness at the nano-scale is an enormous advantage when comparing the corrosion process of different samples. The advantage of AFM is monitoring of roughness before and after exposure and changes in the composition when the surface roughness increases with coating and laser treatments. The hardness of each specimen was measured using a micro-Vickers hardness apparatus at the Department of Production Engineering and Metallurgy, University of Technology. The macro-Vickers hardness was measured using the following formula:

$$H_v = 1.8544 \frac{p}{(dav)^2} \quad (1)$$

where:
P = The applied load =0.5 Kgf, Dav = The average diameter of the two diagonal lengths of the rhombus indentation. A series of readings were taken on the face of the samples, from the outer to the inner diameter.

2.4.2 Analysis of corrosion behavior

Electrochemical work was conducted with potentiostatic polarisation. All tests were performed in 3.5% NaCl solution at room temperature using a computer-controlled potentiostatic instrument (PCI41/750, GAMRYs Instruments, Inc., Warminster, P.A). The Ag/AgCl electrode as reference electrode and Pt auxiliary electrode were used.

The cell contained platinum foil as an auxiliary electrode, the reference was a saturated calomel electrode, and the sample was the working electrode (WE). The holder sported samples as the WE, and the exposed area was 10 mm^2 from one side.

The working temperature was maintained at room-temperature monitoring by a thermometer. No significant change in the temperature was observed during the procedure. First, when the sample was fixed in the WE, the potential difference between the WE and reference electrode was measured by open-circuit polarisation without polarizing the reference electrode.

To apply the Tafel equation, we used the tangent line for the cathode and anode curve automatically by program fitting. The point cross of both lines expressed the corrosion current density (icorr). For cycling, the polarised anode curve for the experimental period will exhibit looping due to the breakdown of the protective film. The point of the cross loop was expressed as a pitting current density. Cell current measurements were obtained during slow screening. The range was from -800 mV to +1900 mV. The scan rate was defined as the speed of 2 mV/s from the potential sweep. The current density to voltage ratio in this context was nearly straight. Experimental findings were determined using the program Echem Analyst.

3. Results and discussion

3.1. Microstructures

The microstructures of the top surface and cross-section of the LC surface of EPD coating were carefully examined by SEM to understand the effects of surface cladding and remelting on the surface characteristics. Figures 2(A, B and C) show the representative scanning electron micrographs of the coating top surface developed by Al_2O_3 with 10% Ni and TiO_2 with 10% Ni and the same remelted surface that followed. A comparison of the surface microstructure of the alloyed zone with melted LC sample coating showed that the coating produced with laser treatment had a relatively smoother top surface, as shown by AFM Figures 7 and 2 (A, B and C), compared with that remelted with laser treatment. This finding was verified by measurement, and comparison of surface roughness parameters (maximum and average) of the two types of surfaces was

performed using a surface profilometer. The remelted coating had distinct globular and acicular particles, which significantly differed from that of the coating treated by laser clad coating. The coating was predominantly a uniform dispersion of small ~300 nm columnar structure and globular titanium-rich phases in an aluminum-rich matrix. These globular and acicular fine particles were identified to be TiO2 and Al2O3, respectively. One of the main important visions was that columnar crystals grew along the direction of heat flow and were not the only type of microstructure that characterises the remelted volume. The formation of fine equiaxed grains in the laser treatment process of ceramic coating was also possible. The phenomena below have been recognised: laser treatment of nanostructured coatings and the surfaces with laser treatment obtaining the desired performance. Analysis of coatings by EDS via revealed more phases, compounds and more detailed information.

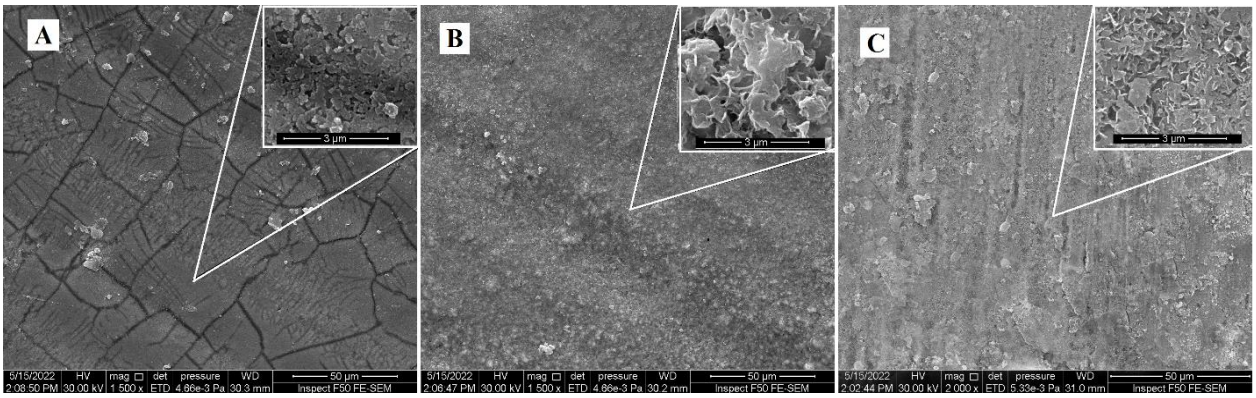

Figure 2. FE-SEM micrograph of the top surface of two representative coatings; (A) laser remelting, (B) Al_2O_3 with 10%, Nickle and (Ni) (B) TiO_2 with 10% Nickle (Ni) laser cladding (C) with laser treatment

The coatings produced by combined EPD and laser surface cladding possessed a fine-grained and semi-amorphous compact microstructure, as shown in the scanning electron micrograph of the ion-milled top surface in Figure 3. Meanwhile, the thickness of the coating prepared by EPD + laser surface cladding was in the range of 11–23 µm, and that of the remelted layers was between 13–26 µm (Figure 3).

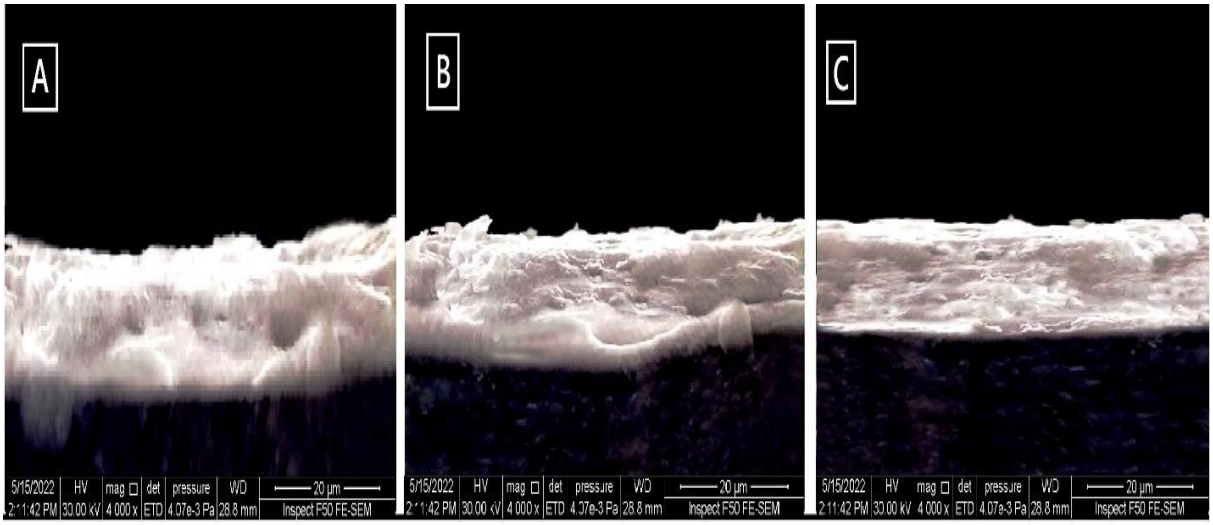

Figure 3. Scanning electron micrograph of the cross-section of the coating with laser

3.2 X-ray diffraction XRD

Figure 4 shows the representative XRD patterns of coatings developed by combined $Al_2O_3$10Ni and $TiO_2$10Ni and laser surface alloying and the same coating followed by laser surface remelting (Figure 4(A)). From the XRD profiles, Al_2O_3, Al_2NiO_4, $FeNi_3$ and Al_2FeO_4 phases were present in the coatings prepared by LC treatment (Figure 4(B)). Figure 4(C) shows the TiO_2 $TiNi_3$, $FeNi_3$ and $TiNiO_3$ in the coatings with LC treatment.

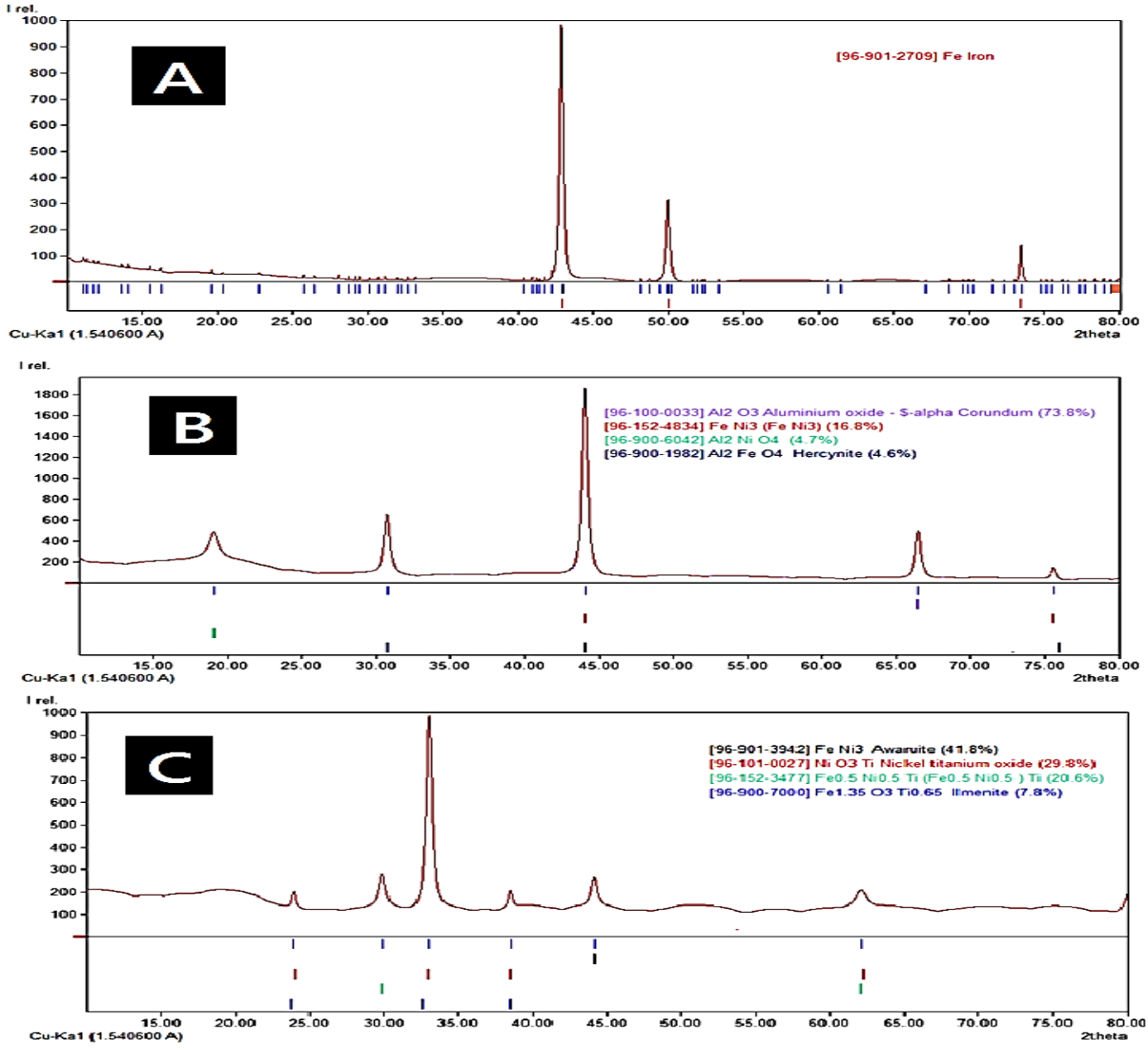

Figure 4. X-ray diffraction patterns of the top surface of (A) laser remelting, (B) Al_2O_3 with 10% Nickle and (Ni) (C) TiO2 with 10% Nickle (Ni) laser cladding

3.3 EDS Analysis

Figure 5(A) exhibits a microstructure with globular and acicular Ti-rich phases dispersed uniformly in the Fe-rich matrix. The top of the coating is shown in Figure 5(B). Data obtained from EDS analysis revealed that the white particles were rich in Ti, and the dark particles were rich in iron and oxygen. However, EDS did not fully identify the elements inside the small particles. Figure 5(C) shows the presence of light elements, including iron, manganese, carbon and silicon, which were accurately indicated by EDS. From the support information obtained from XRD, the white particles were iron and TiO2, whereas the dark patches were Al2O3.

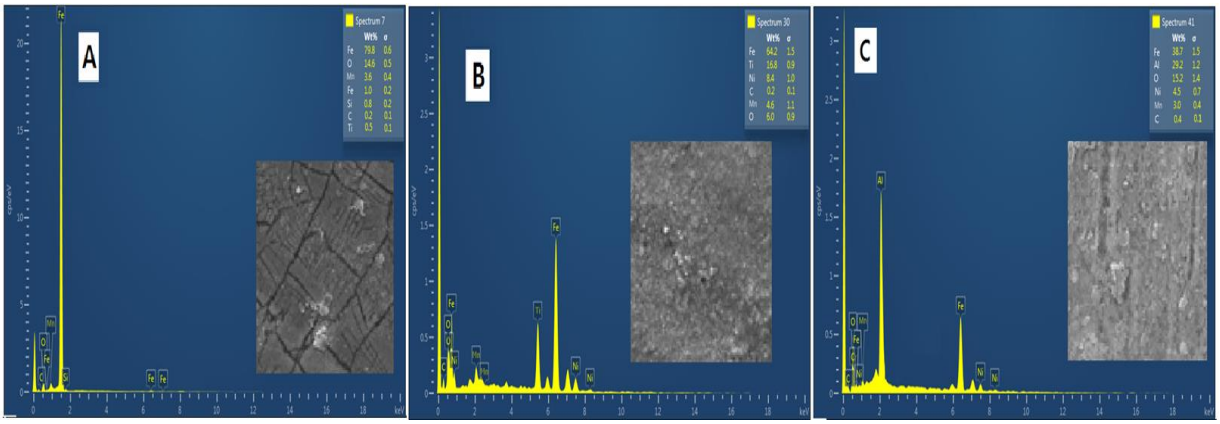

Figure 5. SEM and EDS of the top surface of (A) laser remelting, (B) Al_2O_3 +10%Ni (C) TiO_2+10%Ni laser cladding

3.4 Corrosion behavior

The black line in Figure 6 reveals the corrosion behaviour of remelted A283 low-carbon steel, and the red and blue lines explain the coating-alloy laser-surface cladding. The results showed the corrosion rates of the laser surface cladding toward the noble direction and a protection range greater than that of the remelted steel. In addition, laser surface treatment caused a considerable increase in the corrosion resistance of the steel compared with the base specimen owing to the formation of a passive layer, which represents the corrosion-resistant phase. The results of cyclic tests showed a reasonable decrease in the corrosion rate of the steel after laser surface cladding process. The corrosion resistance of the low-carbon steel after laser treatment of the surface increased considerably due to the electrical conductivity of the passive layer in the solution. Here, the ions present reacted easily with the oxygen of the passive layer. The corrosion rates after laser surface cladding were lower than that obtained after remelting due to the protective alloying layer that formed on the surface. This layer improved the corrosion resistance. The decrease in corrosion rate and the appearance of the protective layer can be explained as the cladding solidification of metal surface in which the precipitates (alloying elements) were dissolved and redistributed in the ordinal alloying matrix, as indicated by rapid melting and re-solidification. Therefore, the surface obtained after laser surface cladding was mostly free from alloying elements. Moreover, a more homogenous microstructure was obtained.

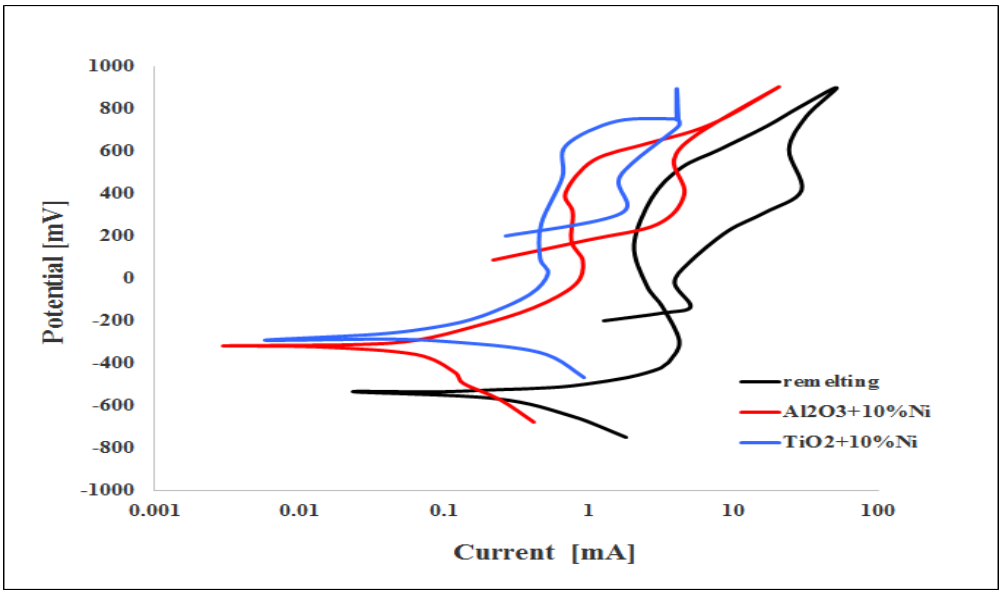

Figure 6. The corrosion behavior for A283 steel for (remelting, Al_2O_3+.10% NI & TiO_2+10%NI)

3.5 AFM investigation

AFM analysis of laser surface cladding coating showed that the topography at the nanoscale was regular and homogenous. This finding was confirmed by the low range of dark areas, which described the low fraction of defects on this scale. The cell sizes within the alloy were very fine, corresponding to the high cooling rate. The solidification micromorphology of alloys during laser surface cladding was observed by advanced AFM analysis (Figure 7). We postulated the nature of shadow effect obtained from the differences between hills and valleys.

The distribution of cell invariants inside the remelted coating suggested a high cooling rate with relatively homogenous distribution of invariants in the range of 87.7 nm (Figure 7A). Figures 7B and 7C also show that the invariants inside the cells after LC were organised in different shapes from spherical to elongate. This finding was due to the localised difference in the cooling rate obtained from the heterogeneous nature distribution. The nano roughness measurements were considerably lower in the laser surface cladding coatings for Al_2O_3+.10% Ni (29.6) and TiO_2+10%Ni (17.8) claddings compared with the remelted surface. AFM analysis of the solidification of laser surface cladding coating confirmed the absence of shadow effect, very low roughness and absence of defects.

The roughness of surface film during remelting and after laser surface cladding was determined by AFM (Figure 7). The AFM image revealed that a rough film formed on the steel surface after laser surface cladding, and it decreased compared with that of the remelted surface. This result was due to the new layer created on the surface because of fast melting and resolidification, whereas the high melting point of oxide increased the surface roughness. Spherical or semi-spherical types of this layer were observed.

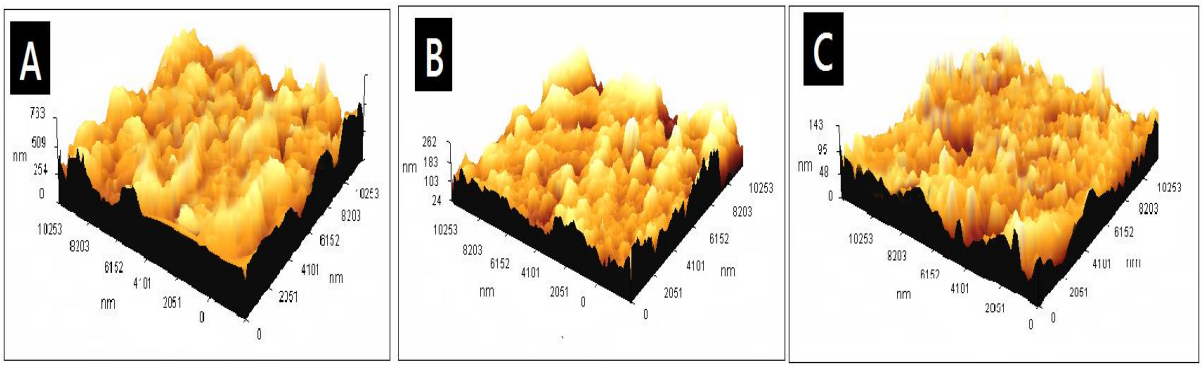

Figure 7. AFM image of laser surface treatments of A283 steel for (A) remelting, (B) Al_2O_3+.10% Ni and (C) TiO_2+10%Ni

3.6 Hardness test

Figure 8 shows the Vickers micro-hardness testing results. Comparing the results with the hardness of A283 steel with laser remelting treatment at 129 HV and that obtained after laser surface cladding, the hardness of the laser surface cladding surface was greater than that of the remelted surface. The increased surface hardness was due to continued dissolution of Al_2O_3 with 10% Ni and TiO_2 with 10% Ni LC from pearlite, and the local minimum was associated with a semi-amorphous structure.

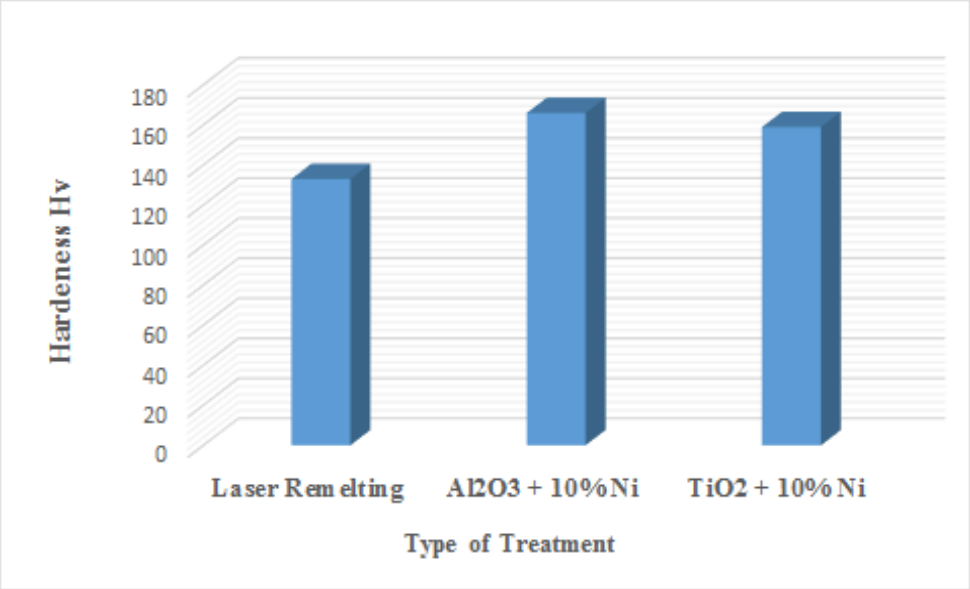

Figure 8. The Vickers micro-hardness testing results

4. Conclusion

Through our investigation of A283 steel We investigated A283 steel produced using a pulsed LC technology. The technology uses electrodeposition technology as a pure-material covering process with control of the particle size and uniform distribution of particles. The laser surface treatment resulted in the following:

- Increased wear resistance of A283 steel after re-melting and during cladding.
- Significantly increased hardness for both processes.
- Quasi-crystalline micro-structures of the coating; crack-free coatings have been obtained with a fine metallic bond to the substrate.
- Improved surface roughness after laser treatment.
- Distribution of casting elements and phases in an orderly manner
- Successful electrodeposition, which is compatible with the use of lasers in cladding operations.

References

[1] P. Schaaf, "Laser Nitriding in Materials," Prog. Mater. Sci., vol. 47, pp. 1–161, 2002.

[2] J. Dutta Majumdar and I. Manna, "Laser material processing," Int. Mater. Rev., vol. 56, no. 5–6, pp. 341–388, 2011, doi: 10.1179/1743280411Y.0000000003.

[3] A. Kruusing, "Underwater and water-assisted laser processing: Part 1 - General features, steam cleaning and shock processing," Opt. Lasers Eng., vol. 41, no. 2, pp. 307–327, 2004, doi: 10.1016/S0143-8166(02)00142-2.

[4] C. S. Montross, T. Wei, L. Ye, G. Clark, and Y. W. Mai, "Laser shock processing and its effects on microstructure and properties of metal alloys: A review," Int. J. Fatigue, vol. 24, no. 10, pp. 1021–1036, 2002, doi: 10.1016/S0142-1123(02)00022-1.

[5] B. N. Mordyuk et al., "Characterization of ultrasonically peened and laser-shock peened surface layers of AISI 321 stainless steel," Surf. Coatings Technol., vol. 202, no. 19, pp. 4875–4883, 2008, doi: 10.1016/j.surfcoat.2008.04.080.

[6] Q. Sulaiman, A. Al Taie, and D. M. Hassan, "Evaluation of Sodium Chloride and Acidity Effect on Corrosion of Buried Carbon Steel Pipeline in Iraqi Soil," vol. 15, no. 1, pp. 1–8, 2014.

[7] M. M. Stack, S. M. Abdelrahman, and B. D. Jana, "Some perspectives on modelling the effect of temperature on the erosioncorrosion of Fe in aqueous conditions," Tribol. Int., vol. 43, no. 12, pp. 2279–2297, 2010, doi: 10.1016/j.triboint.2010.07.015.

[8] N. Andrews, L. Giourntas, A. M. Galloway, and A. Pearson, "Effect of impact angle on the slurry erosion-corrosion of Stellite 6 and SS316," Wear, vol. 320, no. 1, pp. 143–151, 2014, doi: 10.1016/j.wear.2014.08.006.

[9] M. A. Islam and Z. N. Farhat, "The synergistic effect between erosion and corrosion of API pipeline in

CO2 and saline medium," Tribol. Int., vol. 68, pp. 26–34, 2013, doi: 10.1016/j.triboint.2012.10.026.

[10] K. K. Alaneme, M. O. Bodunrin, and S. R. Oke, "Processing, alloy composition and phase transition effect on the mechanical and corrosion properties of high entropy alloys: A review," J. Mater. Res. Technol., vol. 5, no. 4, pp. 384–393, 2016, doi: 10.1016/j.jmrt.2016.03.004.

[11] S. A. Umoren and U. M. Eduok, "Application of carbohydrate polymers as corrosion inhibitors for metal substrates in different media: A review," Carbohydr. Polym., vol. 140, pp. 314–341, 2016, doi: 10.1016/j.carbpol.2015.12.038.

[12] A. Mohammed Nor, M. F. Suhor, M. F. Mohamed, M. Singer, and S. Nesic, "Corrosion of carbon steel in high CO 2 containing environments - The effect of high flow rate," NACE - International Corrosion Conference Series, vol. 7. pp. 5340–5351, 2012.

[13] L. Zeng, G. A. Zhang, and X. P. Guo, "Erosion-corrosion at different locations of X65 carbon steel elbow," Corros. Sci., vol. 85, pp. 318–330, 2014, doi: 10.1016/j.corsci.2014.04.045.

[14] L. Zumofen, A. Kirchheim, and H. J. Dennig, "Laser powder bed fusion of 30CrNiMo8 steel for quenching and tempering: examination of the processability and mechanical properties," Prog. Addit. Manuf., vol. 5, no. 1, pp. 75–81, 2020, doi: 10.1007/s40964-020-00121-x.

[15] Z. Dhib, N. Guermazi, M. Gaspérini, and N. Haddar, "Cladding of low-carbon steel to austenitic stainless steel by hot-roll bonding: Microstructure and mechanical properties before and after welding," Mater. Sci. Eng. A, vol. 656, pp. 130–141, 2016, doi: 10.1016/j.msea.2015.12.088.